Journal of Materials Chemistry A

Accepted Manuscript

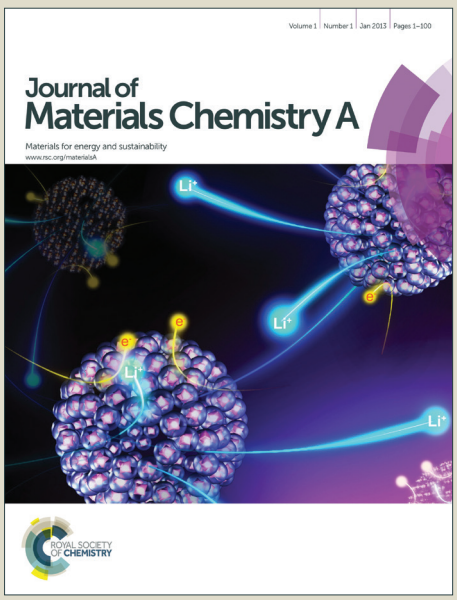

ROYAL SOCIETY OF CHEMISTRY

www.rsc.org/materialsA

Journal Name

RSCPublishing

ARTICLE

Three-Dimensional Superhydrophobic Surface-enhanced Raman Spectroscopy Substrate for Sensitive Detection of Pollutants in Real Environments using an Oil-Water Separation System

Cite this: DOI: 10.1039/x0xx00000x

Received 00th January 2012,
Accepted 00th January 2012

DOI: 10.1039/x0xx00000x

www.rsc.org/

Hongyue Zhao,[a] Jing Jin,[a] Weijun Tian,[b] Ran Li,[a] Zhi Yu,[b] Wei Song,[a]* Qian Cong,[b] Bing Zhao,[a] Yukihiro Ozaki[c]

Despite much effort to improve the design of surface-enhanced Raman spectroscopy (SERS) substrates, it remains a great challenge to develop a general substrate that can separate, enrich, and detect diverse targets in real environments. We demonstrate a novel three-dimensional (3D) superhydrophobic SERS substrate to detect polycyclic aromatic hydrocarbon (PAH) pollutants. The unique 3D superhydrophobic SERS substrate was produced by a galvanic replacement reaction between nickel foam and auric chloride acid, followed by modification with long-chain alkyl mercaptan molecules. Owing to the 3D micro-nanoscale hierarchical structure and long-chain alkyl mercaptan molecules, the as-prepared 3D Au nanoparticles/nickel foam (Au NP/nickel foam) exhibited superhydrophobic properties, which may be used to detect PAHs due to the hydrophobic interactions. In SERS spectra with this substrate, pyrene could be detected at concentrations as low as 10^{-8} M. The enhancement factor of the 3D SERS substrate for pyrene detection was calculated to be about 1.2×10^{4}. This 3D hydrophobic SERS substrate enables the ultrasensitive detection of various analytes with poor affinity for adsorption on conventional SERS substrates, making SERS to a potential and more widely practical analytical technique. Moreover, such 3D hydrophobic SERS substrates could be applied as an oil-water separation system for the separation, enrichment and sensitive detection of pollutants in real environments.

Introduction

Surface-enhanced Raman spectroscopy (SERS) has attracted much attention and has been widely applied in recent years, because it is a powerful tool for the detection of various analytes, with high sensitivity and excellent selectivity in comparison to conventional Raman spectroscopy.[1-5] Noble metals (Au, Ag, and Cu) have been used to fabricate conventional SERS substrates. Colloids, with well-dispersed nanoparticles of noble metals, can be produced for SERS applications by conducting reduction reactions of appropriate solutions with sodium citrate.[6,7] Although such colloids are easily aggregated or precipitated, their synthesis is an intricate process, requiring control of the reaction temperature and the amount of reactants. To overcome the difficulties in the fabrication of SERS substrates and maintain the enhanced effects of noble metals, new synthetic methods are required. In the last decade, many research groups have developed a range of strategies such as sol-gel,[1,8] template,[9] electron beam lithography,[10] oblique angle vapor deposition,[11] and electrodeposition/electrocorrosion[12] methods to fabricate new types of SERS substrates. Among those SERS substrates, porous metallic structures are highly desirable for the detection of diverse analytes in terms of high sensitivity, good reproducibility, and preferable stability.[13-18]

Generally, strong SERS signals are produced only when the analytes have a strong affinity toward a SERS substrate. Thus, it is a great challenge to detect molecules that lack this strong surface affinity. For example, it is difficult to detect polycyclic aromatic hydrocarbons (PAHs) by SERS due to their low affinity to metallic surfaces. PAHs are well known to be carcinogenic, and are common organic contaminants to which the skin, lungs, etc., can be potentially exposed. For sensitive detection of PAHs by a SERS technique, it is necessary to promote the interaction between PAHs and the surface of the substrate. There are some recent reports on the detection of PAHs by SERS, based on the functionalization of the metal surface to bring PAHs into a closer interaction.[19-25] For example, viologen functionalized Ag nanoparticles have been used as SERS substrate to detect PAHs in interparticle hot spots with a high sensitivity.[25] As most PAHs are soluble in organic solvents, but have low solubility in water, it is important to

separate and enrich them before SERS detection in a real environments. Therefore, we have attempted to construct a three-dimensional (3D) SERS substrate based on gold nanoparticles supported on a nickel foam (Au NPs/nickel foam) that possess both superhydrophobic and superoleophilic properties; this substrate can be used as an oil-water separation system for the enrichment and sensitive detection of pollutants in a real environment.

Wettability is a significant property of the solid surface[26-28] and a superhydrophobic surface is usually defined that a water droplet has a contact angle of greater than 150° and a slide angle of less than 10°. Superhydrophobicity of a surface is favored by a low surface energy and a micro-nanoscale hierarchical structure.[29-36] Typically, there are two ways to fabricate the superhydrophobic surface; firstly, the construction of a micro-nanoscale hierarchical structure,[37,38] and secondly, the modification of the surface of a solid with low surface energy molecules.[39,40] Long-chain alkyl mercaptans are a class of molecule commonly used to lower surface energy, which are usually modified on the surface of the micro-nanoscale hierarchical structure to obtain a superhydrophobic surface. Au and Ag nanoparticles interact with the sulfhydryl group, allowing the alkyl chains to arrange in the hydrophobic structure.[41] The superhydrophobic surface is an ideal host material to detect various types of molecules based on their hydrophobic interactions.

In this study, we demonstrate a simple way to fabricate a 3D superhydrophobic SERS substrate for the detection of PAHs. Taking advantage of the 3D structure of Au NPs/nickel foams and the hydrophobic interactions between the 3D structure and the PAHs,[42,43] the enrichment and high sensitive detection of diverse target analytes could be achieved. Moreover, the superhydrophobic and superoleophilic properties of 3D Au NPs/nickel foams enable the separation of oil/water mixtures. Therefore, such a 3D hydrophobic SERS substrate can be used as an oil-water separation system for the enrichment and sensitive detection of pollutants in a real environment.

Experimental section

Materials.

1-octadecanethiol, pyrene and 1-naphthol were purchased from Sigma-Aldrich. Auric chloride acid ($HAuCl_4$) and all the solvents used were obtained from Beijing Chemical Reagent co. Nickel foam was purchased from Changsha LiRun New Materials co.

Fabrication of 3D Au NPs/nickel foam.

Nickel foams were soaked by a concentrated ammonia aqueous solution for 30 min at ambient temperature. The oxide on the surface of nickel foam can be dissolved by the concentrated ammonia aqueous solution with rendering metallic luster. To remove the redundant concentrated ammonia in the gap of nickel foam, rinsing by much more deionized water was necessary. Then, nickel foams were soaked in a $HAuCl_4$ solution with a concentration of 0.001 M to deposit Au nanoparticles on the surface of nickel foam by a galvanic replacement reaction. After the reaction, the color of nickel foam changed from silvery white to golden brown.

Fabrication of 3D Au NPs/nickel foam modified with 1-octadecanethiol.

The as-prepared 3D Au NPs/nickel foam substrates were immersed in a 10^{-3} M ethanol solution of 1-octadecanethiol. The 1-octadecanethiol molecules can arrange on the surface of as-prepared substrates with chemical absorption to form hydrophobic surface. Then, the substrate was washed by a large amount of ethanol to remove the surplus 1-octadecanethiol with physical absorption, and dried in a flow of nitrogen gas.

Sample preparation for SERS measurement.

The modified substrates were immersed in different concentrations of pyrene analytes (from 10^{-3} to 10^{-8} M), with the solvent of chloroform. After immersion, the substrate can be dried at ambient temperature, and then it was used for SERS measurement directly.

Characterization.

Scanning electron microscope (SEM) was used to characterize the morphologies of the as-prepared SERS substrates at 3.0 kV. X-ray photoelectron spectroscopy (XPS) data were taken from a Thermo ESCALAB 250 photoelectron spectrometer with Al Kα X-ray radiation. Raman spectra were measured with by a LabRAM ARAMIS SmartRaman Spectrometer with a HeNe laser as the excitation line of 633 nm. Data acquisition time was 30 s accumulation for one substrate. The Raman band of a Si wafer at 520.7 cm-1 was used to calibrate the spectrometer. The contact angles were obtained from a Dataphysics OCA20 contact-angle system at ambient temperature. The water (about 3.0 μL) droplets were dropped carefully onto the modified samples. The average contact angle value was taken by measuring five different positions of the same sample.

Results and discussion

Fabrication process and morphologies of the 3D hydrophobic SERS substrate

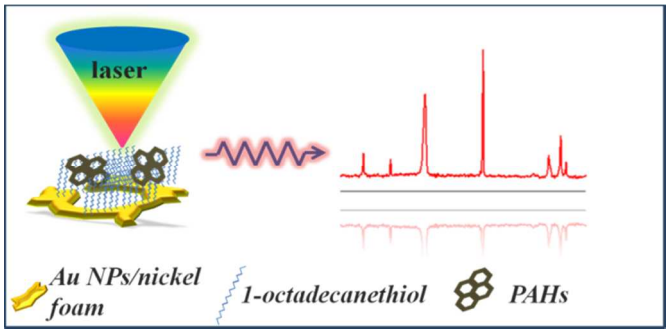

Scheme 1. Schematic illustration for the fabrication process of the 3D hydrophobic SERS substrate and its application to the detection of PAHs.

Scheme 1 illustrates the fabrication of the 3D hydrophobic SERS substrate and detection of PAHs. Au nanoparticles were evenly deposited on the surface of nickel foam in a $HAuCl_4$ solution by galvanic replacement to form a Au NPs/Ni foam. The surface of the as-prepared Au NPs/nickel foam was then decorated with long-chain alkyl mercaptan molecules to obtain the 3D superhydrophobic SERS substrate.

Photographs before and after the galvanic replacement reaction (Insets, Fig. 1a and b, respectively) confirm the deposition of the Au nanoparticles on the surface of the nickel foam, the color of the nickel foam changed from silvery white to golden brown after the galvanic reaction. SEM images show the detailed microstructure of the as-prepared Au NPs/nickel foam. Compared with the smooth surface of the naked nickel foam (Fig. 1a), the surface obtained following the galvanic reaction showed greater roughness owing to the deposition of the Au nanoparticles (Fig. 1b).

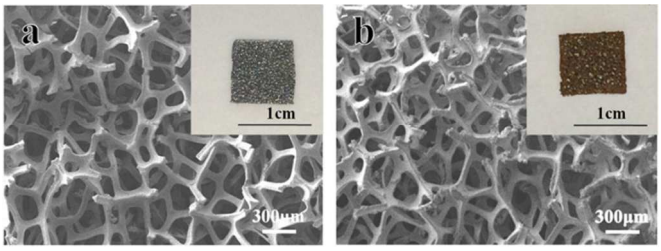

Figure 1. SEM images of (a) the nickel foam and (b) the as-prepared Au NPs/nickel foam. The insets in each panel are the photos of the samples, respectively.

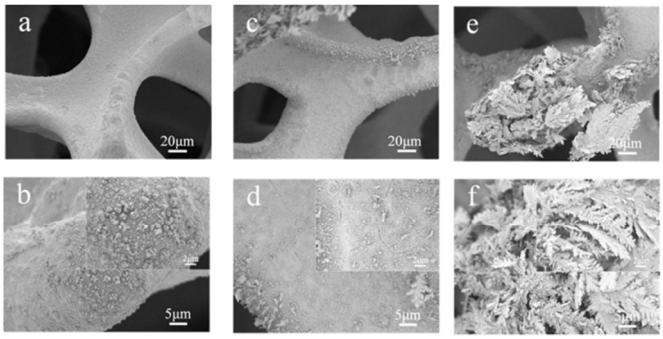

Figure 2. High-magnification SEM images of nickel foam with the deposited gold nanoparticles with 10 min (a, b), 30 min (c, d), and 60 min (e, f). The insets in each panel are the enlargement, respectively.

We have also studied the influence of the reaction time on the morphologies of the as-prepared Au NPs/nickel foam. Fig. 2 displays the SEM images of the Au nanoparticles deposited on the surface of nickel foam with reaction times of 10, 30, and 60 min, respectively. It is evident that the Au nanoparticles increased in size and abundance with increasing reaction time. For a reaction time of 10 min, the branches of nickel foam appear smooth in the low-magnification SEM image (Fig. 2a). However, at higher magnification a small number of Au nanoparticle aggregations are evident on the branches of the nickel foam (Fig. 2b). With a reaction time of 30 min, a mass of Au nanoparticles aggregated on the edges of the branches of the nickel foam (Fig. 2c); the highest density of aggregations was in the middle of the branches (Fig. 2d). Some Au nanoparticles continued to grow and form clubbed and sheet structures (Inset, Fig. 2d). Interestingly, the Au nanoparticles grew gradually larger to produce leafy profiles when the replacement reaction time was increased to 60 min (Fig. 2e). At higher magnification (Fig. 2f), these leafy profiles can be seen clearly, and are observed to overlap together on the raised part of the nickel foam.

Structure characterization and wetting properties of the 3D hydrophobic SERS substrate

The chemical composition of the as-prepared Au NPs/nickel foam was characterized by XPS measurements (Fig. 3). The Au $4f_{7/2}$ and Au $4f_{5/2}$ peaks are observed at about 84.0 and 87.7 eV, respectively (Fig. 3b), clearly demonstrating the presence of Au on the surface of substrate after the galvanic replacement reaction. Peaks at about 855.5 and 873.1 eV are observed in the Ni 2p region (Fig. 3c). Compared with Ni (0) (852.6 eV), these Ni 2p peaks possess higher binding energy, indicating the possible presence of Ni^{2+}. The satellite peaks and poor intensity in the spectra (Fig. 3c) observed in the high binding energy region are also indicative of Ni^{2+}.[44,45] The O 1s peak is evident at 531.1 eV (Fig. 3d), confirming the existence of O^{2-}. It can be concluded that a certain amount of oxide was present on the surface of the nickel foam.

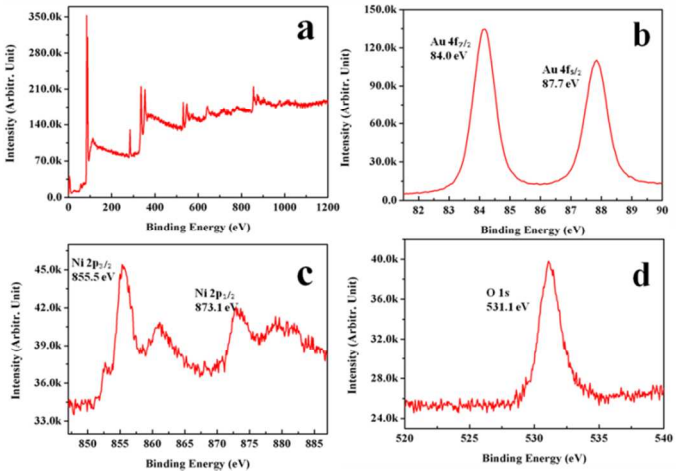

Figure 3. (a) Wide scan XPS spectra of 3D Au NPs/nickel foam. (b) The Au 4f region of 3D Au NPs/nickel foam. (c) The Ni 2p region of 3D Au NPs/nickel foam. (d) The O 1s region of 3D Au NPs/nickel foam.

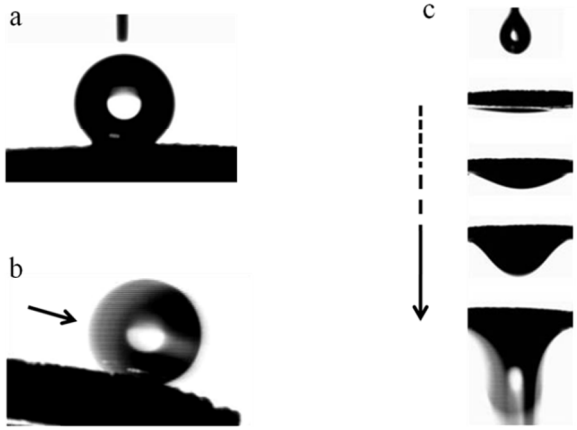

Figure 4. The as-prepared 3D SERS substrate modified by long-chain alkyl mercaptan molecules to show superhydrophobic and superoleophilic properties. (a) Shape of a water droplet (about 3μL) on the modified nickel foam; with the contact angle of about 152.9°. (b) The dynamic behavior of a water droplet on the modified nickel foam, the sliding angle,

about 10°. (c) The chloroform droplet can spread quickly and permeate over the substrate freely.

Long-chain alkyl mercaptan molecules were used to modify the as-prepared 3D Au NP/nickel foam substrates in order to obtain the unique wettability and afford the surface of the substrate with both superhydrophobic and superoleophilic characteristics.[46-48] Fig. 4a illustrates the shape of a water droplet (about 3 μL) on the modified Au NP/nickel foam. The water contact angle was about 152.9° ± 1.1°, demonstrating that the surface of the substrate exhibited superhydrophobicity. The slide angle of about 10° (Fig. 4b) is also indicative of superhydrophobicity. On the surface of the modified Au NP/nickel foam, the water droplets were unstable and could roll off freely. This specific superhydrophobic property results from the micro-nanoscale hierarchical structure and the modification with long-chain alkyl mercaptan molecules. Fig. 4c depicts the spreading and permeating behavior of chloroform droplets on the modified substrates, with a chloroform contact angle of nearly 0°. The chloroform droplets can spread quickly and permeate freely within 1 s. When more chloroform droplets were dropped onto the surface of the modified Au NP/nickel foam, they can spread out and drop off the substrate. This special phenomenon shows that the modified 3D Au NP/nickel foam exhibits superoleophilic characteristics in addition to superhydrophobicity, which is very important for the detection of hydrophobic molecules.[29,49]

The superhydrophobic and superoleophilic properties of the as-prepared 3D Au NPs/nickel foam enable it to be used for the separation of oil/water mixtures. As shown in Fig. S1, chloroform-water and benzene-water separation experiments were performed. The 3D Au NPs/nickel foam was put in the tip of a syringe, and the chloroform/water or benzene/water mixture was placed in it. Because of the superhydrophobic and superoleophilic properties of the 3D Au NPs/nickel foam, chloroform or benzene could pass through the 3D Au NPs/nickel foam and was collected in a vial below, while water remained above the 3D Au NPs/nickel foam. No external pressure was applied during the separation process. From Fig. S1a, it is evident that chloroform could quickly pass through the 3D Au NPs/nickel foam because it is greater than that of water. When the benzene/water mixture was separated, a pipe was employed to facilitate the passage of benzene through the 3D Au NPs/nickel foam, although benzene is lighter than that of water (Fig. S1b).

SERS spectra of PAHs on the modified 3D Au NP/nickel foam substrate

To observe the signals of pyrene from the 3D Au NP/nickel foam substrate modified with 1-octadecanethiol, the SERS spectra of the substrate with chloroform and the substrate with a 10^{-3} M solution of pyrene in chloroform have been studied. It can be clearly seen from Fig. S2 that pyrene molecules could be obviously detected on the surface of the substrate of 1-octadecanethiol-modified 3D Au NP/nickel foam. The density and thickness of Au nanoparticles on the surface of the nickel foam could influence the SERS enhancement effect of the substrates. In this work, the chosen concentration of the $HAuCl_4$ solution for Au nanoparticle deposition was 10^{-3} M. The Au nanoparticles grew uniformly on the surface of nickel foam under such conditions and their density could be controlled by the reaction time. Fig. 5 showed the SERS spectra of pyrene (10^{-3} M) on the 1-octadecanethiol-modified 3D Au NPs/nickel foam substrates with different densities of Au nanoparticles. It was found that the SERS intensity increases with the increased density of Au nanoparticles.

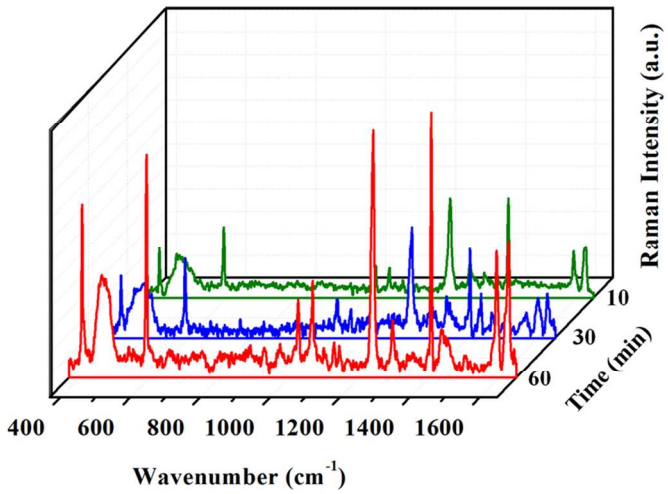

Figure 5. SERS spectra of 10^{-3} M pyrene on the 1-octadecanethiol modified 3D Au NP/nickel foam substrate with the different replacement time (10, 30 and 60 min). The concentration of $HAuCl_4$: 0.001 M.

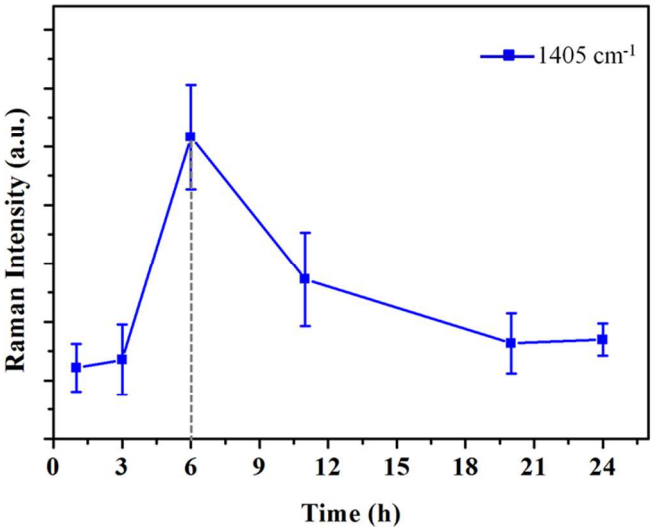

Figure 6. The SERS intensity of the pyrene marker band at 1405 cm^{-1} versus the time of soaking in the 1-octadecanethiol solution. Each error bar means the standard deviation at five different detected positions randomly.

It is well known that the arrangement mode and density of 1-octadecanethiol molecules are changed by controlling the immersion time of the metallic substrate in the 1-octadecanethiol solution. The number of 1-octadecanethiol molecules on the surface of metallic substrates can influence the interaction between the 1-octadecanethiol molecules and PAH molecules, and thus influence the detection of PAHs. As shown in Fig. 6, with increasing immersion time, the Raman intensity at 1405 cm^{-1} (CC stretching/ring stretching) due to pyrene first increases, and then decreases. The Raman intensity reached a peak for an immersion time of 6 h. With a shorter immersion time, the 1-octadecanethiol molecules are arranged sparsely on the surface of the Au NPs/nickel foam. On the

incomplete layer of 1-octadecanethiol, the adsorption of PAH molecules is not maximized, and the corresponding SERS signals are less than maximum intensity. However, when the immersion time is greater than 6 h, the 1-octadecanethiol molecules can arrange to form a denser monolayer. The increased separation of the PAH molecules from the metal surface reduces the surface-enhancement effect, and the resultant SERS signal is weaker.

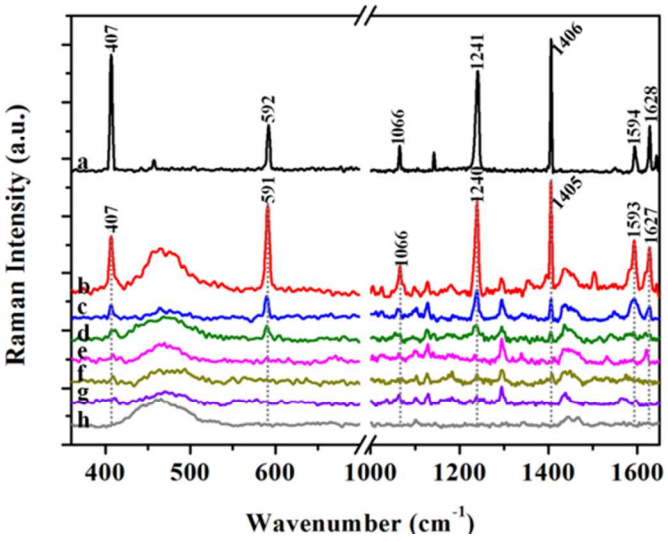

Figure 7. (a) A Raman spectrum of pyrene solid powder, (b)-(g) SERS spectra of pyrene with different concentrations by using the modified substrates: 10^{-3}, 10^{-4}, 10^{-5}, 10^{-6}, 10^{-7} and 10^{-8} M , (h) A Raman specturm of the modified substrate without pyrene.

Fig. 7 exhibits the SERS spectra of different concentrations of pyrene on the surface of the 3D Au NP/nickel foam, and demonstrates that the substrates are suitable for the detection of PAH molecules. Even for pyrene concentrations as low as 10^{-8} M, the peaks at 407 (skeletal stretching), 1066 (CH in-plane bending), 1241 (CC stretching/CH in-plane bending), 1594 cm^{-1} (CC stretching) can still be seen clearly,[24] although, their relative intensities are much weaker than those obtained at higher concentrations.

The dependence of the SERS intensity at 407, 1240, and 1405 cm^{-1} on the concentration of pyrene on the surface of 3D Au NP/nickel foam substrate is shown in Fig. 8. The SERS intensity of each discriminant peak decreases with pyrene concentration, showing a similar trend. The 3D Au NP/nickel foam can also be used as the SERS substrate to detect other types of PAH derivatives, in addition to pyrene. Fig. S3 and S4 show the SERS spectra of 1-naphthol on the surface of the 1-octadecanethiol-modified 3D Au NP/nickel foam, with peaks at 576, 712, 1385, and 1457 cm^{-1} clearly attributable to 1-naphthol. As in the case of 1-naphthol detection, the SERS intensity of the bands at 712 and 1385 cm^{-1} decreases with the decreasing 1-naphthol concentration (Fig. S5). Concentrations of 1-naphthol as low as 10^{-6} M can be detected using the 3D Au NP/nickel foam as the SERS substrate.

Enhancement factor of the modified substrate

The enhancement factor (*EF*) can be defined as[49,50]:

$$EF = (I_{surf}/N_{surf})/(I_{bulk}/N_{bulk})$$

where I_{surf} and I_{bulk} represent the integrated intensities of the equivalent bands of the detected molecule in SERS and conventional Raman spectra, respectively, and N_{surf} and N_{bulk} represent the corresponding number of molecules effectively located in the region of laser beam in the SER and conventional

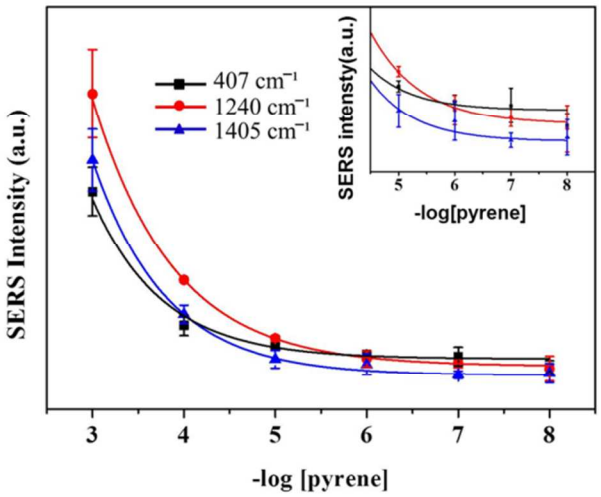

Figure 8. SERS intensity at 1405, 1240 and 407 cm^{-1} versus the concentration of pyrene on the 1-octadecanethiol modified 3D Au NP/nickel foam substrate. The enlargement shows the concentration range of 5-8 of pyrene on the 1-octadecanethiol modified 3D Au NP/nickel foam substrate. Each error bar means the standard deviation at five different detected positions randomly.

Raman spectroscopy experiments, respectively. N_{surf} can be obtained from the equation:

$$N_{surf} = \frac{Ac_{surf}VN_A}{A'}$$

where A is the area of laser spot, c_{surf} is the concentration of the analyte (here, c_{surf} is 10^{-5} M), V is the volume dropped on the surface of the modified substrate (here, V is 20 μL), N_A is the Avogadro constant, and A' is the area of the modified substrate (here, A' is 1 cm^2).

N_{bulk} can be obtained by the equation:

$$N_{bulk} = Ahc_{bulk}N_A$$

The c_{bulk} value can be gained from the molar mass and density of the solid analyte ($c_{bulk} = \frac{\rho(g/cm^3)}{M(g/mol)}$). The effective layer depth of laser penetration, h, can be calculated according to the confocal feature of the microscope. Within the effective depth, each molecule makes a contribution to the Raman signal that is the same as the ideal focal plane.[50,51] We assume that all molecules within the effective depth contribute to the whole Raman signal, and therefore, ignore the Raman signal from outside of the effective depth. The effective depth can be estimated to be 17 μm (1.7×10^{-3} cm). The molecular weight and solid density of pyrene are 202.26 g/mol and 1.271 g/cm^3, respectively. The intensity of 591 cm^{-1} band was used to calculate the value of the enhancement factor. The normal Raman and SERS spectra were measured under the same acquisition time, excitation wavenumber, and laser power. In conclusion, a value of about 1.2×10^4 was obtained for the EF using the 1-octadecanethiol-modified Au NP/nickel foam substrate.

Application of the 3D hydrophobic Au NPs/nickel foam SERS substrate

As the 3D hydrophobic SERS substrate with unique superhydrophobic and superoleophilic properties can be obtained on the surface of nickel foam, we can fabricate an oil-water separation and pollution detection apparatus using this special phenomenon. Scheme 2 illustrates such a system. As shown in Fig. S6, a mixture of organic solvents with the PAH analytes and aqueous solution of salt or a contaminant can be separated by the oil-water separation system. The aqueous solution containing the salt and contaminant cannot flow through the Au NP/nickel foam due to its superhydrophobicity. However, the organic solvent with the PAH analytes does flow through. The hydrophobic interaction between PAHs and 1-octadecanethiol results in the adsorption of PAH molecules on the surface of the modified 3D Au NP/nickel foam. After the completion of the separation step, the 3D hydrophobic substrate can be extracted for SERS measurements. Thus, we have created a simple measurement system to detect pollutants in real environment by the SERS technique.

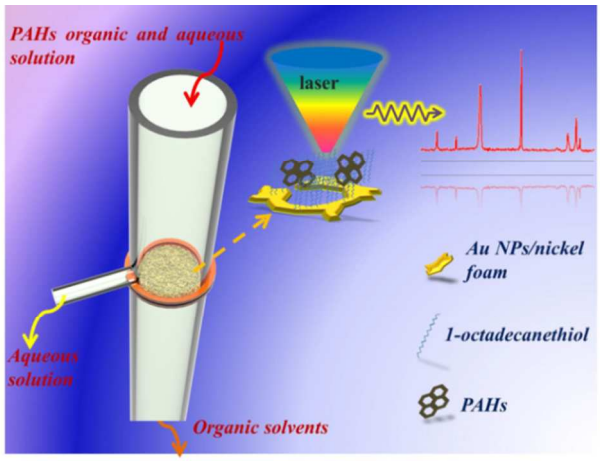

Scheme 2. Schematic illustration for the oil-water separation and pollution detection system with the 3D hydrophobic SERS substrate.

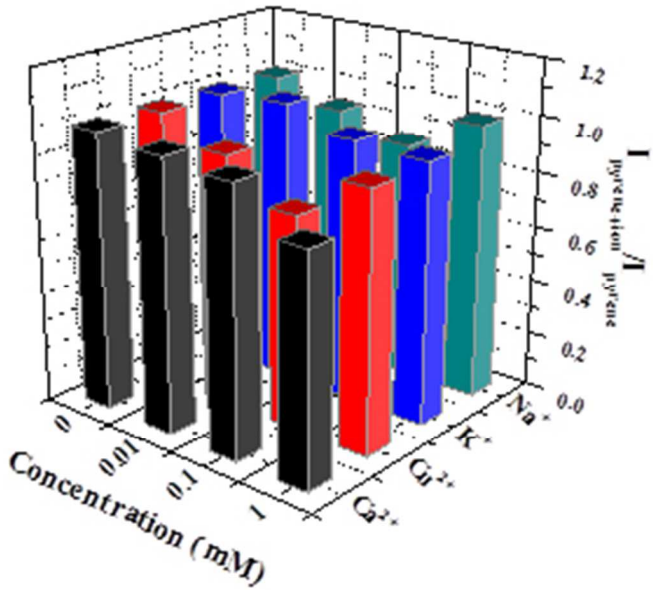

Figure 9. Histograms of the integrated relative intensities at 1405 $cm^{-1}$of the pyrene solution with metal ions (Na^+, K^+, Cu^{2+} and Ca^{2+}) and the pyrene solution without metal ions. The data of intensities are the average values at five different positions.

Compared with other SERS substrates such as silver and gold sol, the 3D Au NP/nickel foam substrate has a lower propensity toward aggregation of small nanoparticles, showing an enhanced chemical and structural stability. In addition, the 3D Au NP/nickel foam is superhydrophobic and acts as an oil-water separation system to detect pollutants in a real environment; it can simultaneously separate, enrich, and detect the pollutants in the real environment quickly and efficiently. In order to investigate the possibility of interference by metal ions in real environments, we tested the simple device for the detection of pyrene molecules in solutions with different concentrations of metal ions (Na^+, K^+, Cu^{2+}, and Ca^{2+}). Pyrene (1 mM) and metal ion solution with different concentrations (0.01, 0.1, and 1 mM) were mixed in an equal volume ratio, and passed through the 3D hydrophobic SERS substrate to allow the adsorption of pyrene molecules. As shown in Fig. S7 and Fig. 9, there is little change to the integrated relative intensities of the pyrene bands with changing metal ion (Na^+, K^+, Cu^{2+}, and Ca^{2+}) concentration, indicating that the metal ions have little influence on the detection of PAHs. Therefore, the simple device can be used to quickly detect the hydrophobic molecules in the organic solvent with no need to remove the interference from metal ions. In order to verify the detection of PAHs and their derivatives through the SERS technique in real environment, we have tested the SERS spectra of pyrene and 1-naphthol molecules on the surface of modified 3D Au NP/nickel foam in the tap water, which have been shown in Fig. S8 and S9. Moreover, the recovery percent was also calculated and summarized in Table S1 and S2. These results indicated that the superhydrophobic 3D Au NP/nickel foam could act as SERS substrate to detect pollutants in a real environment.

Conclusions

In summary, we have proposed a 3D SERS substrate with superhydrophobic and superoleophilic properties. The substrate could be used as an oil-water separation system for the enrichment and sensitive detection of pollutants in real environments, with measurements over the concentration range of 10^{-3}–10^{-8} M. The 3D SERS substrate can be simply and rapidly synthesized without a complicated preparation process. The surface of nickel foam with a micro-nanoscale hierarchical structure, on which Au nanoparticles had been deposited, was modified with 1-octadecanethiol molecules to produce a superhydrophobic and superoleophilic substrate. The hydrophobic interaction between 1-octadecanethiol and PAHs molecules allowed adsorption and detection of PAHs at concentrations as low as 10^{-8} M. The modified 3D Au NP/nickel foam can detect various kinds of PAHs and their derivatives, including pyrene and 1-naphthol. It is expected that this type of substrate can also be applied to the detection of a wide variety of hydrophobic molecules.

Ackowledgement

This work was supported by the National Natural Science Foundation of China (No. 20903044, 21273091, 21327803, 21473068), the Development Program of the Science and Technology of Jilin Province (20130522137JH). We also thank Mr. Ziyi Cheng for his kindly help for the schematic illustration.

Notes and references

[a] State Key Laboratory of Supramolecular Structure and Materials, Jilin University; 2699#,Qianjin Steet, Changchun 130012, P. R. China
[b] Key Laboratory for Terrain – Machine Bionics Engineering Mimistry of Education, Jilin University; 5988#, Renmin Street, Changchun 130025, P.R. China
[c] School of Science and Technology, Kwansei Gakuin Universty, 2-1 Gakuen, Sanda, Hyogo 660-1337, Japan

† Electronic Supplementary Information (ESI) available: [details of any supplementary information available should be included here]. See DOI: 10.1039/b000000x/

1 S. Nie and S. R. Emory, *Science*, 1997, **275**, 1102–1106.
2 G. McNay, D. Eustace, W. E. Smith, K. Faulds and D. Graham, *Applied Spectroscopy*, 2011, **65**, 825–837.
3 K. Hering, D. Cialla, K. Ackermann, T. Dörfer, R. Möller, P. Rösch and J. Popp, *Anal Bioanal Chem*, 2008, **390**, 113–124.
4 S. M. Asiala and Z. D. Schultz, *Analyst*, 2011, **136**, 4472–4479.
5 R. Kodiyath, J. Wang, Z. A. Combs, S. Chang, M. K. Gupta, K. D. Anderson, R. J. Brown and V. V. Tsukruk, *Small*, 2011, **7**, 3452–3457.
6 P. C. Lee and D. Meisel, *J. Phys. Chem.*, 1982, **86**, 3391–3395.
7 G. Frens, *Nature Physical Science*, 1973, **241**, 20–22.
8 C. J. Murphy, T. K. San, A. M. Gole, C. J. Orendorff, J. X. Gao, L. Gou, S. E. Hunyadi and T. Li, *J. Phys. Chem. B* 2005, **109**, 13857-13870.
9 W. D. Ruan, C. X. Wang, N. Ji, Z. C. Lu, T. L. Zhou, B. Zhao and J. R. Lombardi, *Langmuir*, 2009, **24**, 8417-8420.
10 Y. J. Liu, Z. Y. Zhang, Q. Zhao, R. A. Dluhy and Y. P. Zhao, *Appl. Phys. Lett.*, 2009, **94**, 0331033.
11 J. D. Driskell, S. Shanmukh, Y. J. Liu, S. B. Chaney, X. J. Tang, Y. P. Zhao and R. A. Dluhy, *J. Phys. Chem. C*, 2008, **112**, 895-901.
12 S. K. Yang, D. Slotcavage, J. D. Mai, F. Guo, S. X. Li, Y. H. Zhao, Y. Lei, C. E. Cameron and T. J. Huang, *J. Mater. Chem. C*, 2014, **2**, 8350-8356.
13 S. Chan, S. Kwon, T. W. Koo, L. P. Lee, A. A. Berlin, *Adv. Mater.*, 2003, **15**, 1595-1598.
14 L. H. Lu, A. Eychmüller, *Acc. Chem. Res.*, 2008, **41**, 244-253.
15 S. J. Lee, A. R. Morrill, M. Moskovits, *J. Am. Chem. Soc.*, 2008, **128**, 2200-2201.
16 H. Ko, S. Chang, V. V. Tsukruk, *ACS Nano*, 2009, **3**, 181-188.
17 X. Y. Xiao, J. Nogan, T. Beechem. G. A. Montano, C. M. Washburn, J. Wang, S. M. Brozik, D. R. Wheeler, D. B. Burckel, R. Polsky, *Chem. Commun.*, 2011, **47**, 9858-9860.
18 C. Fang, A. V. Ellis, N. H. Voelcker, *J. Electroanal. Chem.*, 2011, **659**, 151-160.
19 C. E. Taylor, M. H. Schoenfisch and J. E. Pemberton, *Langmuir*, 2000, **16**, 2902–2906.
20 J. C. S. Costa, A. C. Sant'Ana, P. Corio and M. L. A. Temperini, *Talanta*, 2006, **70**, 1011–1016.
21 L. Guerrini, J. V. Garcia-Ramos, C. Domingo and S. Sanchez-Cortes, *Anal. Chem.*, 2009, **81**, 953–960.
22 L. Guerrini, J. V. Garcia-Ramos, C. Domingo and S. Sanchez-Cortes, *J. Phys. Chem. C*, 2008, **112**, 7527–7530.
23 C. L. Jones, K. C. Bantz and C. L. Haynes, *Anal. Bioanal. Chem.*, 2009, **394**, 303–311.
24 Y. F. Xie, X. Wang, X. X. Han, X. X. Xue, W. Ji, Z. H. Qi, J. Q. Liu, B. Zhao and Y. Ozaki, *Analyst*, 2010, **135**, 1389-1394.
25 L. Guerrini, J. V. Garcia-Ramos, C. Domingo, S. Sanchez-Cortes, *Anal. Chem.*, 2009, **81**, 1418-1425.
26 R. S. Subramanian, N. Moumen and J. B. Mclaughlin, *Langmuir*, 2005, **21**, 11844–11849.
27 N. Moumen, R. S. Subramanian and J. B. McLaughlin, *Langmuir*, 2006, **22**, 2682–2690.
28 A. Uyama, S. Yamazoe, S. Shigematsu, M. Morimoto, S. Yokojima, H. Mayama, Y. Kojima, S. Nakamura and K. Uchida, *Langmuir*, 2011, **27**, 6395–6400.
29 X. X. Zhang, L. Wang and E. Levänen, *RSC Adv.*, 2013, **3**, 12003–12020.
30 C. F. Wang, S. F. Chiou, F. H. Ko, C. T. Chou, H. C. Lin, C. F. Huang and F. C. Chang, *Macromol. Rapid Commun*, 2006, **27**, 333–337.
31 S. T. Wang, Y. L. Song and L. Jiang, *Nanotechnology*, 2007, **18**, 015103.
32 L. Feng, Z. Y. Zhang, Z. H. Mai, Y. M. Ma, B. Q. Liu, L. Jiang and D. B. Zhu, *Angew. Chem. Int. Ed.*, 2004, **43**, 2012–2014.
33 M. Kiuru and E. Alakoski, Mater. Lett., 2004, 58, 2213–2216.
34 W. J. Fang, H. Mayama and K. J. Tsujii, *Phys. Chem. B*, 2007, **111**, 564–571.
35 M. Nicolas, F. Guittard, S. Ge´ribaldi, *Langmuir*, 2006, **22**, 3081–3088.
36 H. Yabu, M. Takebayashi, M. Tanaka and M. Shimomura, *Langmuir*, 2005, **21**, 3235–3237.
37 M. J. Liu, Y. M. Zheng, J. Zhai and L. Jiang, *Accounts of Chemical Research*, 2010, **43**, 368–377.
38 B. J. Li, M. Zhou, W. Zhang, G. Amoako, C. Y. Gao, *Applied Surface Science*, 2012, **263**, 45–49.
39 Y. W. Su; B. H. Ji, Y. G. Huang and K. C. Hwang, *Langmuir*, 2010, **26**, 18926–18937.
40 D. Varshney, V. I. Makarov, P. Saxena, A. González-Berríos, J. F. Scott, B. R. Weiner and G. Morell, *Nanotechnology*, 2010, **21**, 285301.
41 H. L. Zhang, M. Chen and H. L. Li, *J. Phys. Chem. B*, 2000, **104**, 28–36.
42 C. M. Zhao, X. Wang, S. Wang, H. X. Wang, Y. C. Yang and W. T. Zheng, *Materials Research Bulletin*, 2013, **48**, 3189–3195.
43 X. M. Hou, X. L. Zhang, S. T. Chen, H. Z. Kang and W. H. Tan, *Colloids and Surfaces A: Physicochem. Eng. Aspects*, 2012, **403**, 148–154.
44 A. F. Carley, S. D. Jackson, J. N. O'Shea and M. W. Roberts, *Phys. Chem. Chem. Phys.*, 2001, **3**, 274–281.
45 P. R. Sajanlal and T. Pradeep, *Nanoscale*, 2012, **4**, 3427–3455.
46 W. Song, J. J. Zhang, Y. F. Xie, Q. Cong and B. Zhao, *J. Colloid Interface Sci.*, 2009, **329**, 208-211.
47 L. Feng, Z. Y. Zhang, Z. H. Mai, Y. M. Ma, B. Q. Liu, L. Jiang and D. B. Zhu, *Angew. Chem. Int. Ed.* 2004, **43**, 2012–2014.
48 M. Kiuru, E. Alakoski, *Materials Letters*, 2004, **58**, 2213–2216.
49 Y. F. Xie, X. Wang, X. X. Han, W. Song, W. D. Ruan, J. Q. Liu, B. Zhao and Y. Ozaki, *J. Raman Spectrosc.*, 2011, **42**, 945–950.

50 H. Y. Jia, J. B. Zeng, W. Song, J. An and B. Zhao, *Thin Solid Films*, 2006, **496**, 281–287.
51 W. B. Cai, B. Ren, X.Q. Li, C.X. She, F.M. Liu, X.W. Cai and Z.Q. Tian, *Surface Science*, 1998, **406**, 9–22.

Graphical Abstract

A unique three-dimensional superhydrophobic Surface-enhanced Raman spectroscopy substrate has been developed, which could be fabricated as a novel oil-water separation system for the enrichment and sensitive detection of pollutants in a real environment.